Journal of Geophysical Research: Space Physics

RESEARCH ARTICLE
10.1029/2018JA025626

North-South Asymmetric Kelvin-Helmholtz Instability and Induced Reconnection at the Earth's Magnetospheric Flanks

S. Fadanelli[1,2], M. Faganello[3], F. Califano[1], S. S. Cerri[4], F. Pegoraro[1], and B. Lavraud[2]

[1]Dipartimento di Fisica "E. Fermi", Università di Pisa, Pisa, Italy, [2]IRAP, Université de Toulouse, CNRS, CNES, UPS, (Toulouse), France, [3]Aix-Marseille University, CNRS, Marseille, France, [4]Department of Astrophysical Sciences, Princeton University, Princeton, NJ, USA

Key Points:
- Three-dimensional two-fluid simulations including of Kelvin-Helmholtz instability including high-latitude stabilization
- Detailed analysis of the north-south asymmetric development of the Kelvin-Helmholtz instability
- Detailed analysis of the north-south asymmetric development of magnetic reconnection induced by the Kelvin-Helmholtz vortices

Correspondence to:
M. Faganello,
matteo.faganello@univ-amu.fr

Citation:
Fadanelli, S., Faganello, M., Califano, F., Cerri, S. S., Pegoraro, F., & Lavraud, B. (2018). North-south asymmetric Kelvin-Helmholtz instability and induced reconnection at the Earth's magnetospheric flanks. *Journal of Geophysical Research: Space Physics*, *123*, 9340–9356. https://doi.org/10.1029/2018JA025626

Received 2 MAY 2018
Accepted 26 SEP 2018
Accepted article online 5 NOV 2018
Published online 22 NOV 2018

Abstract We present a three-dimensional study of the plasma dynamics at the flank magnetopause of the Earth's magnetosphere during mainly northward interplanetary magnetic field periods. Two-fluid simulations show that the initial magnetic shear at the magnetopause and the field line bending caused by the dynamics itself (in a configuration taken as representative of the properties of the flank magnetopause) influence both the location where the Kelvin-Helmholtz (KH) instability and the induced magnetic reconnection take place and their nonlinear development. The KH vortices develop asymmetrically with respect to the Earth's equatorial plane where the local KH linear growth rate is maximal. Vortex-driven reconnection processes take place at different latitudes, ranging from the equatorial plane to midlatitude regions but only in the hemisphere that turns out to be the less KH unstable. These results suggest that KH-induced reconnection is not limited to specific regions around the vortices (inside, below, or above) but may be triggered over a broad and continuous range of locations in the vicinity of the vortices.

1. Introduction

The large-scale dynamics of the Earth's magnetosphere can be modeled, as a first approach, adopting a one-fluid magnetohydrodynamic (MHD) description. In fact the magnetospheric plasma follows an *ideal* dynamics over most of its spatial domain, the magnetic field lines being frozen into the plasma motion and any cross-field diffusion being fairly negligible(Labelle & Treumann, 1988; Le et al., 1994; Sonnerup, 1980). The magnetospheric region where field lines are *anchored* to the Earth is separated from the heated solar wind plasma of the magnetosheath, where the interplanetary magnetic field (IMF) lines are connected to the open space, by a magnetic boundary known as the magnetopause.

Independent of its complex magnetic shape, in the absence of cross-field diffusion the frozen-in law prevents any kind of mixing between the magnetospheric and the solar wind plasmas. Therefore, the plasma of solar wind origin could not in principle enter into the less dense magnetosphere.

However, the frozen-in condition can be locally violated by nonideal effects arising at small scales generated by the plasma dynamics itself, for example, allowing for magnetic reconnection to occur. Since reconnection is capable of modifying the global magnetic field topology, it strongly impacts both the dynamics of the whole system and the transport properties at the magnetopause. In particular, during southward periods when the IMF direction is opposite to that of the magnetospheric magnetic field at low latitude, reconnection occurs at dayside magnetopause allowing for direct transport across the magnetopause and leading to the formation of a low-latitude boundary layer (LLBL) where solar wind and magnetospheric plasmas can mix (Dungey, 1961).

During northward periods the magnetic configuration at the low-latitude magnetopause is unfavorable for magnetic reconnection to occur. Nevertheless, the formation of a LLBL is observed also during these periods (Mitchell et al., 1987) up to the point that the entry of solar wind particles into the magnetosphere can be even more important than during southward periods (Terasawa et al., 1997). Different mechanisms have been invoked for explaining this transport, which is routinely observed by satellites.

The nonlinear vortex dynamics resulting from the development of the Kelvin-Helmholtz (KH) instability is one of the few phenomena, together with lobe reconnection (Gosling et al., 1991; Onsager et al., 2001; Song & Russell, 1992) and kinetic Alfvén waves (Chaston et al., 2007; Johnson & Cheng, 2001; Johnson et al.,

2001), that are able to explain the observed transport (see, e.g., Faganello & Califano, 2017, for further details on the respective role of the different phenomena). The KH instability is driven by the velocity shear between the stagnant magnetosphere and the flowing magnetosheath plasma of solar wind origin and grows along the magnetospheric flanks at low latitude, where the stabilizing magnetic shear is weaker for northward IMF. By contrast, under such northward IMF conditions, higher-latitude regions are instead completely stabilized by the stronger magnetic shear.

Per se, the KH vortices developing during the nonlinear phase can strongly perturb the magnetopause but cannot mix the two different plasmas as their typical scale is so large that their early dynamics remains *MHD ideal*. However, they become the driver of very fast secondary instabilities, which give rise to a rich, small-scale nonlinear dynamics that feeds on the energy source provided by the vortical motion: from secondary KH and Rayleigh-Taylor instabilities (Faganello et al., 2008a; Matsumoto & Hoshino, 2004; Nakamura & Daughton, 2014; Tenerani et al., 2011) to magnetic reconnection (Faganello et al., 2008b; Faganello, Califano, Pegoraro, & Andreussi, 2012; Knoll & Brackbill, 2002; Nakamura et al., 2006; Otto & Fairfield, 2000), magnetorotational instability (Matsumoto & Seki, 2007), or current-sheet kink instability (Nakamura et al., 2004).

If a magnetic shear exists across the low-latitude magnetopause, the KH velocity field will eventually pinch the magnetopause current sheet in between vortices and force the so-called *Type I* vortex-induced reconnection (VIR) to occur there (Liu & Hu, 1988). In this case reconnection must proceed on nearly the same ideal time scale of the vortex dynamics in order to release the magnetic energy that piles up at the compressed current sheet carried by the ideal motion (Chen et al., 1997; Knoll & Brackbill, 2002; Nakamura et al., 2006, 2013). Type I reconnection creates field lines that thread through the magnetopause, leading to a direct entry of solar wind particle into the magnetosphere.

If the initial magnetic shear is set to 0 and high-latitude KH stable region are included in the model, it has been shown that reconnection develops first at midlatitude instead of around the equatorial plane where the vortices are generated by the primary KH instability. This process is driven by the braiding and the stretching of the field lines advected by the vortices at the equator but remaining anchored at higher latitudes in the Earth's magnetosphere (Faganello, Califano, Pegoraro, & Andreussi, 2012, 2014).

Under such conditions, midlatitude reconnection develops almost symmetrically with respect to the equatorial plane and creates double-reconnected flux tubes. These newly closed flux tubes, located on the earthward side of the magnetopause, thus become populated with dense solar wind plasma. In this way, solar wind plasma enters the magnetosphere at a rate that is compatible with the observed one (Faganello, Califano, Pegoraro, & Andreussi, 2012).

Recently, Meteosat microwave sounder (MMS) spacecraft data have provided unambiguous in situ evidence of magnetic reconnection, which were interpreted as Type I reconnection at the compressed current sheets forming in between primary successive KH vortices (Eriksson et al., 2016), confirming past observations with Cluster (Hasegawa et al., 2009; Nykyri et al., 2006). Remarkably, for the same MMS event evidences were also found for remote reconnection (Vernisse et al., 2016), that is, occurring far away from the satellite location, as signaled by heated ions and electrons flowing parallel and antiparallel along magnetic field lines just outside the magnetopause (e.g., Gosling et al., 1991; Fuselier et al., 1995; Lavraud et al., 2006). These results suggest that Type I and midlatitude reconnection coexist and cooperate in forming the LLBL for northward IMF, when a magnetic shear is present.

Here we present a numerical study that takes into account both a preexisting shear between the magnetospheric field and the IMF, as well as the high-latitude stabilization of the KH instability, allowing for the simultaneous development of Type I and midlatitude reconnection. In section 2 we present the plasma model, the initial equilibrium and the parameters used in our simulations. In section 3 we show how the large-scale structures of the vortices are modified when both magnetic shear and high-latitude stabilization are present. In section 4 we present the analysis of the KH-induced reconnection processes. Finally, in section 5 conclusions are drawn.

2. Plasma Model and Simulation Setup

We adopt a Hall-MHD plasma model (including finite resistivity). The model equations, in conservative form, are as follows:

$$\partial_t n + \nabla \cdot (n\mathbf{u}) = 0, \tag{1}$$

$$\partial_t(n\mathbf{u}) + \nabla \cdot \left(n\mathbf{u}\mathbf{u} + P_{tot}\bar{\bar{\mathbf{I}}} - \mathbf{B}\mathbf{B} \right) = \mathbf{0}, \tag{2}$$

$$\partial_t \mathbf{B} = -\nabla \times \mathbf{E}, \tag{3}$$

$$\mathbf{E} = -\mathbf{u} \times \mathbf{B} + \mathbf{J}/n \times \mathbf{B} - \nabla P_e /n + \eta \mathbf{J}, \tag{4}$$

where all quantities are normalized to ion (proton) quantities, the ion mass m_i, the inertial length d_i, and the Alfvèn speed v_A. Here n is the plasma number density, $\mathbf{u} \simeq \mathbf{u}_i$ the fluid velocity and $P_{tot} = P_i + P_e + B^2/2$. The ion and electron thermal pressures are evolved following an ideal adiabatic closure:

$$\partial_t(nS_{i,e}) + \nabla \cdot \left(nS_{i,e}\mathbf{u}_{i,e} \right) = 0 \quad ; \quad S_{i,e} = P_{i,e}n^{-5/3}. \tag{5}$$

Finally, we neglect the displacement current; then, the Faraday equation and the electron fluid velocity are given by

$$\mathbf{J} = \nabla \times \mathbf{B} \quad ; \quad \mathbf{u}_e = \mathbf{u} - \mathbf{J}/n. \tag{6}$$

With this model, during the initial large-scale dynamics leading to the formation of fully rolled-up KH vortices, the magnetic field is frozen into the ion fluid motion and the dynamics is correctly described by ideal MHD. During this phase the system spontaneously starts to distort and shrink the initial current sheet, eventually reaching a characteristic width comparable with the ion inertial length d_i. As a result, where the magnetic configuration is favorable, Hall reconnection sets in on a fast time scale (Birn et al., 2001; Faganello et al., 2008c, 2012). Admittedly, our model neglects the kinetic dynamics at scales smaller than d_i, as well as possible anisotropy effects (see, e.g., Cerri et al., 2013; De Camillis et al., 2016, and references therein). Nevertheless, when implemented for reproducing a large portion of the boundary our model can realistically evaluate reconnection-induced plasma exchanges at the magnetopause (see Henri et al., 2013). Indeed we are not interested in the kinetic details of the reconnecting structures, such as ion and electrons exhausts, particle acceleration or particle streaming along newly reconnected lines but on the modification of the global magnetic topology during the KH evolution. For this purpose a Hall-MHD description is sufficient since it is able to catch the correct reconnection rate and thus to describe correctly the modifications of the global topology during the time-evolving configuration created by the KHI.

The model equations are integrated numerically using a fourth-order Runge-Kutta scheme. Spatial derivatives are calculated using sixth-order explicit finite differences along the periodic y and z directions, while a sixth-order implicit compact scheme with spectral-like resolution (Lele, 1992) is adopted along the inhomogeneous x direction. Very short wavelength fluctuations are dissipated using high-order spectral filters acting only on the high-k part of the spectrum (Lele, 1992).

Special care is devoted to the boundaries along the inhomogeneous x direction where we adopt transparent conditions for any MHD alfvénic or sonic perturbation generated inside the numerical domain. This method is based on projected characteristics of the ideal-MHD set of equations allowing one to control the influx/outflux flux at the boundaries (Faganello et al., 2009; Hedstrom, 1979; Landi et al., 2005; Thompson, 1990). In order to deal with the nonideal MHD terms of our set of equations, such as the Hall and the diamagnetic terms in the Ohm's equation, we gradually smooth them out in a buffer regions close to the boundaries. We set the boundaries far enough from the central region where small-scale structures develop during the dynamics and where nonideal effects are thus important. Thus, we do not observe any spurious reflection neither at the boundaries nor in the buffer regions.

Simulations are initialized starting from a 2-D ideal MHD equilibrium taken as uniform along the flow direction (y coordinate). The x and z axis are set perpendicular to the unperturbed magnetopause and along the northward direction, respectively. In this configuration all equilibrium quantities are functions of ψ only, where $\psi = \psi(x, z)$ is a magnetic flux function satisfying the Grad-Shafranov equations (Andreussi et al., 2012; Faganello, Califano, Pegoraro, & Andreussi, 2012; Faganello, Califano, Pegoraro, Andreussi, Benkadda, et al., 2012).

$$\Delta\psi = \frac{\mathrm{d}}{\mathrm{d}\psi}\Pi \quad ; \quad \Pi = P_{0,i} + P_{0,e} + B_{0,y}^2/2. \tag{7}$$

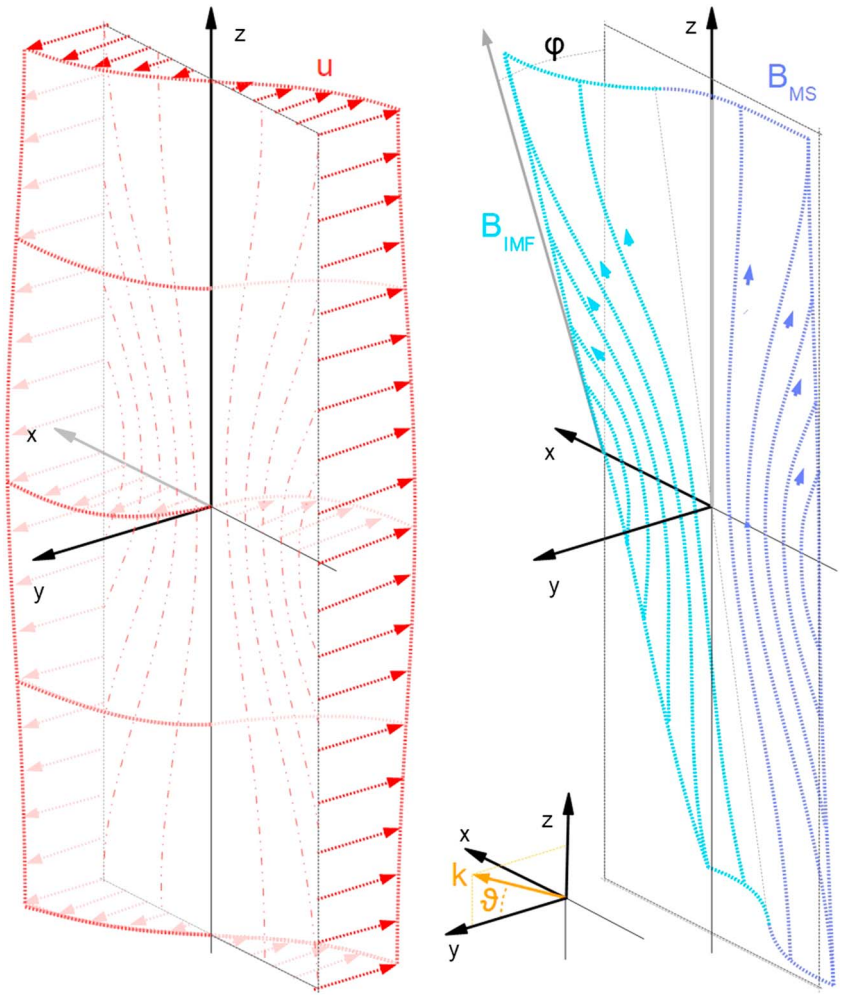

Figure 1. Schematic representation of the magnetic and velocity fields in the equilibrium configuration. φ represents the angle between the IMF and the northward direction $\hat{\mathbf{z}}$. ϑ defines the angle between a given wavevector $\mathbf{k}$ lying in the (y,z) plane and the flow direction $\hat{\mathbf{y}}$. IMF = interplanetary magnetic field.

Setting $\Pi = cst$ a simple solution is given by

$$\psi_0(x,z) = \frac{1+\delta}{2}x + \frac{1-\delta}{2}\frac{L_z}{2\pi}\sinh\frac{2\pi x}{L_z}\cos\frac{2\pi z}{L_z}, \tag{8}$$

while the other equilibrium quantities are set as

$$n_0 = 1, \tag{9}$$

$$\mathbf{u}_0(x,z) = \frac{u_\star}{2}\tanh\frac{\psi_0(x,z)}{\ell_\star}\mathbf{e}_y, \tag{10}$$

$$\mathbf{B}_0(x,z) = \nabla\times\psi_0(x,z)\mathbf{e}_y + \frac{\tan(\varphi)}{2}\left[1+\tanh\frac{\psi_0(x,z)}{\ell_\star}\right]\mathbf{e}_y, \tag{11}$$

where φ is the shear angle between the magnetospheric field and the IMF. The first term in equation (11) corresponds to the northward magnetospheric field ($x<0$) and the dominant northward component of the IMF ($x>0$). The second term adds a flow-aligned component to the IMF, taking into account possible different configurations that are observed during periods of northward IMF. The equilibrium thermal pressure $P_{0,i}+P_{0,e}$ is the dominant term in Π and varies from the magnetosphere to the magnetosheath in order to compensate for the increasing of $B_{0,y}^2/2$. A sketch of this equilibrium configuration is given in Figure 1.

In our simulations we set $L_z = 120\pi$ and $\delta = 1/3$ so that the northward component of the magnetic field is nearly straight inside within the interval $-L_x/2 < x < L_x/2$, with $L_x = 90$. Setting $\ell_\star = 3 \ll L_x$ we obtain

Table 1
Summary of the Relevant Parameters Characterizing the Different Simulations

Run	M_A	M_s	$\tan(\varphi)$	Description
A	1.0	$\sqrt{3/5}$	0.3	weak magnetic shear
B	2.0	$\sqrt{12/5}$	1.0	strong magnetic shear & high velocity

an equilibrium configuration that varies mainly along the x direction and a velocity shear layer vorticity at $x = 0$ that is 3 times larger at $z = 0$ than at $z = \pm L_z/2$. As a consequence the KH instability, whose maximal growth rate is a fraction of the velocity shear layer vorticity (Drazin & Reid, 1981), develops far faster in the equatorial region than at higher latitudes. This initial 2-D configuration permits to mimic the preferential equatorial development of the KH instability at the flank magnetopause, under northward IMF. In the case of the Earth's magnetosphere, however, stabilization at higher latitudes is expected and observed owing to magnetosheath flow and magnetic field draping properties, so that magnetic and flow fields become more aligned and thus less prone to KH development (Chandrasekhar, 1961). The box dimension along the flow is $L_y = 2\lambda_{FGM,z=0} = 30\pi$, where $\lambda_{FGM,z=0}$ is the expected wavelength of the fastest growing mode as given by a simplified 2-D stability analysis at the equatorial plane. The number of grid points along each direction is given by $n_x = 900$, $n_y = 512$, $n_z = 512$.

The sonic and alfvénic Mach number are defined as $M_s = u_\star/c_s$ and $M_A = u_\star/v_{A,z}$, where c_s and $v_{A,z}$ are calculated at at the centre of the numerical box. Their values, together with the other parameters, are listed in Table 1. Finally, we take $P_i = P_e$ and $\eta = 0.001$.

In order to follow the system evolution, to individuate the plasma structures forming during the dynamics and to follow the field line connectivity, we define a passive tracer ς advected by the fluid so as to mark the two different plasmas during the evolution. At the beginning of the simulation the passive tracer is set as

$$\varsigma(x,z) = 0.6 + 0.4\ \tanh\left[\frac{\psi_0(x,z)}{\ell_\star}\right], \tag{12}$$

where $\varsigma < 0.6$ corresponds to the magnetospheric plasma and $\varsigma > 0.6$ to the solar wind one, while $\varsigma \simeq 0.6$ determines the position of the magnetopause. The passive tracer ς is constant along each magnetic field line and evolves as the field lines would do within ideal MHD. In this way ς allows us to identify the reconnected lines linking the magnetospheric and solar wind plasma as those along which a variation of ς is measured.

3. Large-Scale Dynamics of KH Vortices

3.1. Overview of the Dynamics

As expected, from the initial white noise perturbation KH waves emerge around the wavelength associated with the fastest-growing mode (FGM) as predicted by linear theory. Given the length of the numerical box, two vortices appear at the end of the linear phase (not shown here). As soon as they enter the nonlinear phase the pairing process starts (Miura, 1997; Winant & Browand, 1974). As a result the vortices eventually merge generating a single larger vortex.

In Figure 2 we show the passive tracer isocontours at $t = 460$ for run *B*. For the sake of clarity, the box has been doubled along the y direction so that two pairs of coupling vortices appear instead of one. The semitransparent quasi-vertical isosurface corresponds to the magnetopause, $\varsigma = 0.6$, while the dark/light blue color correspond to the magnetospheric/solar wind plasma.

Two pairing vortices have been produced around the equatorial region, the magnetopause being wrapped inside the vortex motions. The vortex structures, as shown by the folded magnetopause, extend both into the Northern Hemisphere and into the Southern Hemisphere and are tilted with respect to the z axis, corresponding to a KH wave vector not aligned with the initial flow. We recall that in the absence of an initial magnetic shear ($\tan\varphi = 0$), the KH vortex axis would be parallel to the z axis. As expected for the chosen initial configuration, the vortices grow around the central region of the box while they are stable at high latitudes, as shown by the color configuration in the unperturbed planes at $z = \pm L_z/2$. However, the presence

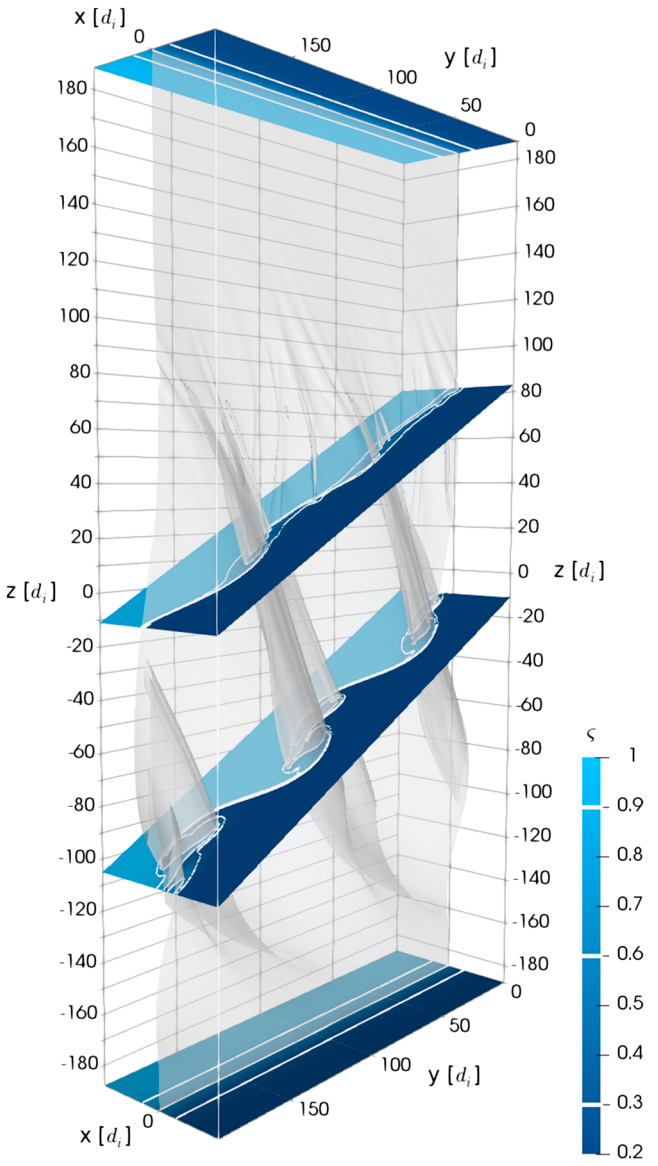

Figure 2. Visual rendering of the instability onset and development for $\tan\varphi = 1.0$ (B simulation) at $t = 460$. The shaded isosurface ($\varsigma = 0.6$) corresponds to the magnetopause while dark/light blue colors correspond to the magnetospheric/solar wind plasmas. The white isocontours correspond to the passive tracer values $\varsigma = 0.3, 0.6, 0.9$. Note that for easing the visualization the box has been doubled along the y direction.

of an equilibrium magnetic shear breaks the reflection symmetry with respect to the equatorial plane of our initial configuration. Indeed, while $\mathbf{u}_0$ and $B_{0,z}$ are symmetric, $B_{0,y} \to -B_{0,y}$ for $z \to -z$: The different properties under reflection follow from the fact that the velocity is a vector while the magnetic field is an axial vector.

As a consequence, vortices develop differently in the Northern and in the Southern Hemispheres, for example, preferring the Southern Hemisphere for $\tan\varphi > 0$ as shown in Figure 2 (the opposite is true for $\tan\varphi < 0$). The physical mechanism that favors one hemisphere with respect to the other is the combined action of vortex growth and field line tying at high latitudes as will be discussed next in section 3.3.

3.2. The Tilting of Unstable Modes

The vortex tilting observed in Figure 2 is the consequence of the presence of a magnetic shear in the equilibrium configuration. This point can be understood as follows. The most unstable modes are the ones able to minimize the magnetic tension proportional to $\mathbf{k}\cdot\mathbf{B}_0$ (that counteracts the KH development) more than to maximize the driving term proportional to $\mathbf{k}\cdot\mathbf{u}_0$ (here $\mathbf{k} = 2\pi m/L_y\mathbf{e}_y + 2\pi n/L_z\mathbf{e}_z$ is the mode wave vector; m and n, the mode numbers along y and z). This effect has been proven to be at work when considering 1-D equilibria varying only along x (Southwood, 1968; Walker, 1981) but remains efficient also in our 2-D equilibria with high-latitude stabilization. Indeed, the most unstable modes underlying the development of the vortex structures have a wave vector oblique with respect to the flow velocity, and it is roughly perpendicular to the magnetic field direction (close to the velocity shear layer).

In order to calculate the KH growth rate analytically, we consider the limit where the flow velocity and the magnetic field are uniform in two different regions separated by a sharp discontinuity at $x = 0$. In our equilibrium configuration this would correspond to the limit $\ell_\star \to 0$ and $\delta \to 1$. By assuming incompressible perturbations, the KH growth rate is given by (Chandrasekhar, 1961)

$$\gamma(k,\vartheta,M_A,\varphi) = k\cos(\vartheta)\left[\frac{M_A^2}{4} - \tan^2\vartheta - \tan\vartheta\,\tan\varphi - \frac{\tan^2\varphi}{2}\right]^{1/2}, \quad (13)$$

where ϑ is the angle between the wave vector and the flow direction $\mathbf{e}_y$. This system is unstable if and only if $\vartheta_- \le \vartheta \le \vartheta_+$, where $\vartheta_\pm$ is defined by

$$\vartheta_\pm = \arctan\left[-\frac{\tan\varphi}{2} \pm \frac{\sqrt{M_A^2 - \tan^2\varphi}}{2}\right]. \quad (14)$$

Once all the parameters but φ are fixed, the most unstable modes are found for

$$2\vartheta_{\max} = -\arctan\left(\frac{4\tan\varphi}{4 - 2\tan^2\varphi + M_A^2}\right) \quad (15)$$

that is different from 0 provided that $\tan\varphi \neq 0$. For small M_A and small φ we have $\vartheta_{\max} \simeq -\varphi/2$, so that $\mathbf{k}\cdot\mathbf{B}_0 = 0$ around the center of the velocity shear layer. For large φ the angle $\vartheta_{\max} < -\varphi/2$ because in our equilibrium configuration the magnitude of $\mathbf{B}_0$ is bigger in the magnetosheath than in the magnetosphere by a factor $(1+(\tan\varphi)^2)^{1/2}$. For large M_A the stabilizing effect of the magnetic field is reduced so that the most unstable wave vector tends to be aligned with the flow ($|\vartheta_{\max}|$ decreases). Note that for $z \to -z$, the magnetic shear angle φ as well as ϑ change sign and that $\gamma(-\vartheta,-\varphi) = \gamma(\vartheta,\varphi)$.

Even if this model is oversimplified, it yet gives some insights about the tilt angle of oblique modes observed in the 3-D compressible simulations starting from 1-D equilibria with $\ell_\star \neq 0$ (Adamson et al., 2016; Nakamura

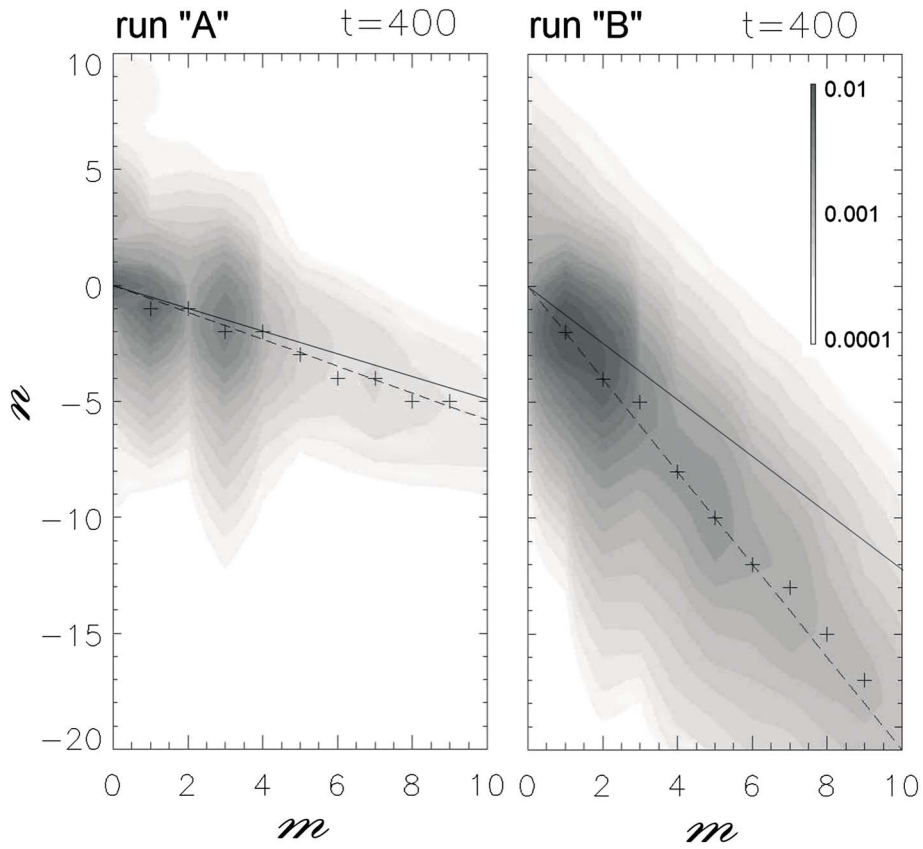

Figure 3. Shaded isocontours of the *x*-averaged Fourier amplitude of u_x, normalized on the characteristic velocity $u_\star$, taken at $t = 400$ for $\tan\vartheta = 0.3$ and $\tan\vartheta = 1.0$, left and right frames, respectively. The continuous lines represent the most unstable modes given by the (n, m) couples as predicted from the analytical step-like configuration. The dashed line by $\vartheta_{\text{shear}} = -\arctan[(\tan\varphi)/2]$. For each discrete m value, a cross indicates the location of maximal amplitude as obtained in simulations. Clearly, crosses are almost aligned along the continuous line.

& Daughton, 2014). A moderate discrepancy between the predicted ϑ_{max} and that observed in the simulations is related to the fact that the simplified model underestimates the role of the magnetic field inside the shear layer ($|x| \lesssim \ell_\star$), where the mode amplitude is larger, while overestimates its importance in the two asymptotic region ($|x| \gg \ell_\star$). This is clearly shown by our simulations where the observed angle of the most unstable modes is slightly smaller than the predicted one. The actual angle, for both runs *A* and *B* is closer to $-\arctan[(\tan\varphi)/2]$ than to ϑ_{max}: The most unstable modes tend to develop perpendicular to the magnetic field at the center of the shear layer, minimizing the stabilizing role of the magnetic tension where the velocity shear term is stronger. Note that, at the center of the shear layer ($x = 0$) the flow-aligned component of the magnetic field is given by $B_{0,y} = \frac{\tan\varphi}{2}$, so that the angle between $\mathbf{B_0}$ and $\mathbf{e}_z$ there is not $\varphi/2$ but $\arctan[(\tan\varphi)/2]$. This is why unstable modes develop preferentially at $\vartheta_{\text{shear}} = -\arctan[(\tan\varphi)/2]$. This is shown in Figure 3 where we plot the magnitude of the *x*-averaged Fourier components of u_x in the (m, n) plane (m and n are the mode numbers as defined before) for $\tan\varphi = 0.3$ and $\tan\varphi = 1.0$. For each m number the largest amplitude correspond to $n < 0$, that is, to a tilted mode. The central region of the most unstable (tilted) modes observed in the simulations (gray strips) is aligned along the direction given by $\vartheta_{\text{shear}} = -\arctan[(\tan\varphi)/2]$ (dashed line), so that $\mathbf{k}\cdot\mathbf{B}_0 \simeq 0$ at the center of the shear layer. On the contrary ϑ_{max} (continuous line) slightly underestimates the tilting. For $\tan\varphi = 0.3$ we have $\vartheta_{\text{max}} \simeq 7°$ and $\vartheta_{\text{shear}} \simeq 8°$. For $\tan\varphi = 1.0$, $\vartheta_{\text{max}} \simeq 17°$ and $\vartheta_{\text{shear}} \simeq 27°$.

3.3. Latitudinal Shift of the Vortices

Due to the presence of the magnetic shear in the equilibrium configuration the large-scale KH vortices extend asymmetrically with respect to the equatorial plane. In particular, for $\tan\varphi > 0$, the latitude band affected by the vortex structures shifts southward, below the equatorial plane. As we will discuss later, the opposite is true

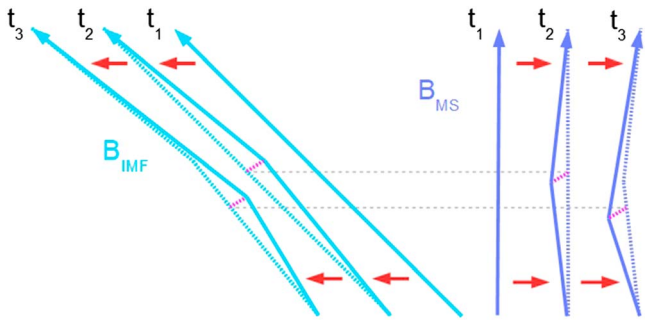

Figure 4. A sketch of the differential magnetic field line advection mechanism for $\tan\varphi > 0$. The figure shows a magnetospheric/IMF line, light blue and dark blue colors, respectively, at three different times. The unperturbed field lines, denoted by t_1, first bend close to the equators, resulting into magnetic field lines at time t_2, due to the different advection at high/low latitudes, that is, field lines move unperturbed in opposite directions at high latitudes while they are slowed down in the equatorial plane. Indeed, as the field lines are frozen into the fluid motion, they are slowed down in the equatorial plane because they are embedded in the vortex structures whose phase velocity is nearly 0. The magnetic shear is thus enhanced in the Northern Hemisphere and reduced in the Southern Hemisphere causing a southward drift of the instability. As a consequence the region where magnetic field lines are slowed down gradually shifts southward, as shown for $t = t_3$, as well as the region with smaller magnetic shear, favoring the KH development. IMF = interplanetary magnetic field.

for $\tan\varphi < 0$. Qualitatively, this vortex shift can be explained by the differential advection of the magnetic field lines with respect to the latitude position.

Differential advection has been discussed in the limit $\tan\varphi = 0$, that is, zero magnetic shear, as an important driver for the magnetic field lines dynamics (Borgogno et al., 2015; Faganello, Califano, Pegoraro, & Andreussi, 2012). Indeed, magnetic field lines embedded in the vortex structures are slowed down in the equatorial region, with respect to their unperturbed motion, since the KH phase velocity is null in our frame. On the contrary they continue to move at the unperturbed magnetosphere/solar wind velocity at high latitudes. As a consequence, magnetic field lines of different origin are stretched and arched in the opposite directions, leading to the formation of intense current sheets at midlatitudes where reconnection finally occurs. When an initial magnetic shear is present, differential advection works somewhat differently. At the beginning the KH mode develops symmetrically with respect to $z = 0$ but as soon as the vortices start to form, differential advection becomes more and more important and, contrary to the case without magnetic shear, modifies the vortex structure in a different way above and below the equatorial plane.

A sketch of this mechanism is given in Figure 4 for $\tan\varphi > 0$. We see that the initial magnetospheric and IMF lines, initially straight at $t = t_1$, are stretched by the differential advection, resulting in magnetic field lines that are increasingly bent at $t = t_2$ and $t = t_3$. As a consequence the magnetic shear is enhanced in the Northern Hemisphere while it is reduced in the Southern Hemisphere. Since the magnetic shear tends to inhibit the KH instability the location of the maximal growth rate gradually drifts southward. As a result, for $\tan\varphi > 0$, the KHI eventually develops faster in the Southern Hemisphere.

The different evolution of the magnetic shear in the two hemispheres can be quantified by looking at the peaks of electric current $J = |\mathbf{J}| = |\nabla \times \mathbf{B}|$. In Figure 5, top frame, we plot $\max_x(\tilde{J}_{m=0}(x,z)) \,/\, \max_x(J_0(x,z))$ as a function of z for $t = 250, 300, 350$, up to the beginning of the nonlinear phase. Here J_0 is the magnitude of the equilibrium current, while $J_{m=0}$ is the magnitude of the $m = 0$ mode of the total current, thus including the nonlinear modification of the equilibrium. It is clear that the $m = 0$ magnetic shear is amplified in the Northern Hemisphere while it lowers in the Southern Hemisphere, explaining the southward shift of the KH unstable region at the beginning of the nonlinear phase.

In the present configuration, where the vorticity $\boldsymbol{\Omega}_0$ associated with the initial sheared flow is along $+\hat{\mathbf{z}}$, the equilibrium current $\mathbf{J}_0$ points out the hemisphere where the magnetic shear becomes larger. In general (for $\Omega_{0,z} \lessgtr 0$), the symmetry properties of the mechanism described in Figure 4 suggest that differential advection enhances the magnetic shear in the Northern Hemisphere for $\boldsymbol{\Omega}_0 \cdot \mathbf{J}_0 > 0$, while the opposite is true for $\boldsymbol{\Omega}_0 \cdot \mathbf{J}_0 < 0$. As a consequence KH vortices develop more vigorously in the Southern/Northern Hemisphere for $\boldsymbol{\Omega}_0 \cdot \mathbf{J}_0 \gtrless 0$.

As a reference, in Figure 5, bottom frame, we plot the normalized value of the peaks of the total current $J = |\mathbf{J}|$ at $t = 350$ as a function of z: $\max_{(x,y)}(J(x,y,z))/\max_x(J_0(x,z))$. The maximal current increases at all latitudes due to the lateral compression of the original current sheet imposed by the KH velocity field. At the same time the current amplification is more important in the Northern Hemisphere than in the Southern Hemisphere because of differential advection.

4. Magnetic Field Line Dynamics

4.1. Overview of the Dynamics

Most field lines maintain their connections during the whole dynamics even if strongly bent and stretched by the KH vortical motion. In particular field lines on the left (right) of the magnetopause isosurface $\varsigma = 0.6$ at $t = 0$ remain on the same side. On the other hand the connections of some field lines, such as the yellow ones drawn in Figure 6, are affected by magnetic reconnection occurring various places at the magnetopause. Now these field lines connect two initially well-separated magnetic domains: left and right of the magnetopause.

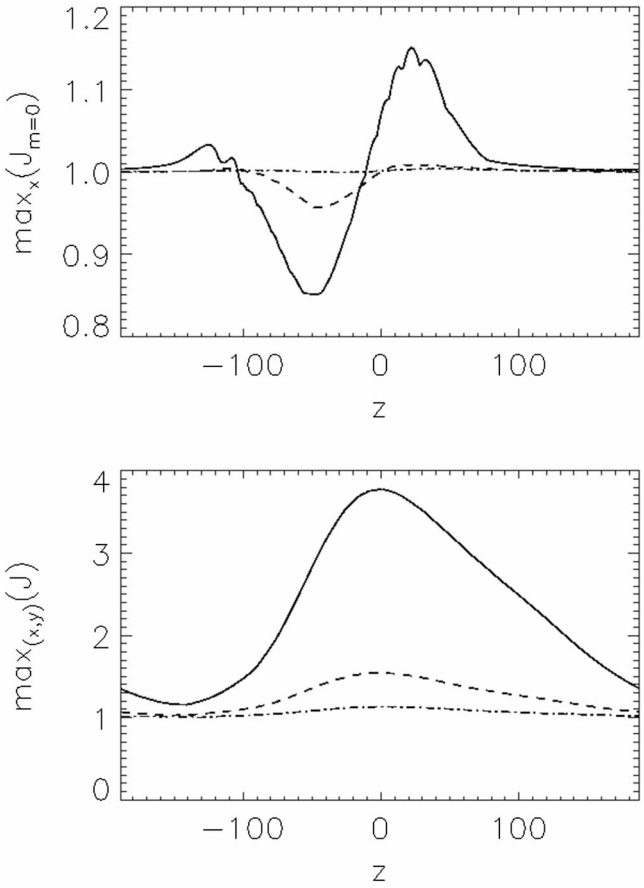

Figure 5. Top frame: $\max_x(\tilde{J}_{m=0}(x,z))/\max_x(J_0(x,z))$ as a function of z at $t = 250, 300, 350$. Bottom frame: $\max_{(x,y)}(J(x,y,z))/\max_x(J_0(x,z))$ at $t = 250$ (dash-dotted), $t = 300$ (dashed), $t = 350$ (continuous).

This is shown in Figure 6, where such magnetic field lines cross the $\varsigma = 0.6$ isosurface at several latitudes, from the magnetosheath (blue) to the magnetosphere (light blue), thereby connecting both sides of the magnetopause.

The dynamics investigated here is more complex than that discussed in Faganello, Califano, Pegoraro, & Andreussi (2012); Faganello, Califano, Pegoraro, Andreussi, Benkadda, et al. (2012, 2014); and Borgogno et al. (2015). It includes at the same time a preexisting magnetic shear between the magnetosheath and the magnetospheric fields and high-latitude stabilization of the KH instability, so that reconnection can occur both as Type I or midlatitude reconnection. The former process is driven by the pinching of the preexisting current sheet caused by the compression in between KH vortices. Therefore, it is expected to locally occur where the instability grows the most (Chen et al., 1997; Knoll & Chacón, 2002; Nakamura et al., 2006). The latter is instead related to the field line differential advection and thus may be triggered at current sheets created (or modified) by this advection, far away from the main location of the KH vortices (Borgogno et al., 2015; Faganello, Califano, Pegoraro, & Andreussi, 2012; Faganello, Califano, Pegoraro, Andreussi, Benkadda, et al., 2012, 2014).

We have shown in Figure 5, bottom frame, that in the presence of a sheared magnetic field with $\tan\varphi > 0$ the combined action of differential advection and lateral compression increases the electric current at all latitudes but in particular in the Northern Hemisphere, that is, in the hemisphere opposite to that where the vortices are most intense. On this basis we may expect that Type I reconnection would preferentially occur around the equatorial region while midlatitude reconnection would be favored in the Northern Hemisphere. In order to understand the development of such a complex dynamics we need to determine a quantity that can act as a proxy for where reconnection occurs.

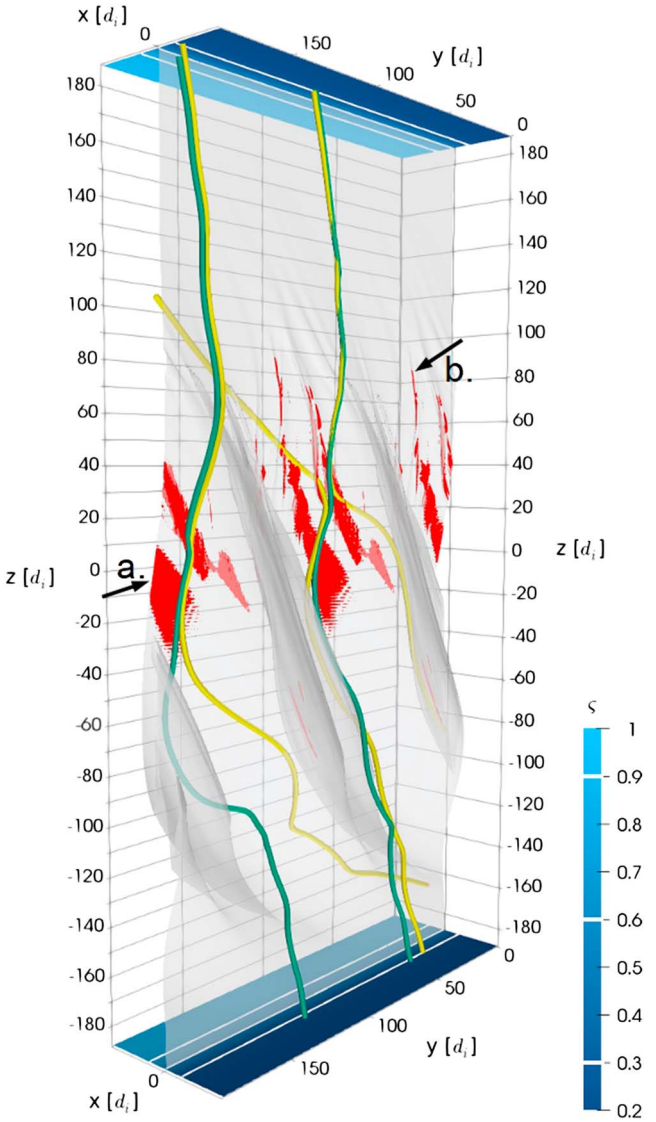

Figure 6. Shaded isosurface ($\varsigma = 0.6$) corresponding to the magnetopause and dark/light blue colors corresponding to the magnetospheric/magnetosheath plasmas for $\tan\varphi = 1.0$ at $t = 460$. The white isocontours correspond to the passive tracer values $\varsigma = 0.3, 0.6, 0.9$. The regions where reconnection takes place are enclosed in the $|\varkappa| > 0.03$ volumes, highlighted in red. The black arrows indicate planar (a) and elongated (b) reconnection sites. Some magnetic field lines representative of those crossing the active reconnecting sites have also been drawn in yellow if reconnected and in green if not. Note that for easing the visualization the box has been doubled along the *y* direction.

4.2. Finding Reconnection: A 3-D Diagnostic

Determining reconnection sites in a full 3-D, time-dependent geometry is far from straightforward. When a preexisting current sheet is present, the current density $|\mathbf{J}|$ and the magnetic shear already have quite *large* values, so they are not very useful when seeking for reconnecting regions. The passive tracer ς defined above (equation (12)) is, instead, a convenient proxy for defining *reconnected* field lines since only along these lines a variation of ς can occur, that is, $\mathbf{B} \cdot \nabla\varsigma \neq 0$. However, such a tracer cannot identify the precise location of ongoing reconnection.

Hence, in order to find reconnection active regions we define the following quantity:

$$\varkappa = (\partial_t + \mathbf{u} \cdot \nabla)(S_e - S_i) = (\mathbf{J} \cdot \nabla S_e)/n\,, \tag{16}$$

where equations (1), (5), and (6) have been used. The idea behind this relies on the fact that in our plasma model the entropy of each species is passively advected by its respective fluid velocity. A difference between

the electron and ion entropy advection thus indicate regions where ions and electrons decouple which, in a Hall reconnection regime, include the reconnection regions. We thus expect that magnetic field lines passing through regions where the value of $|\varkappa|$ peaks are those undergoing reconnection. These may be either magnetic field that have not yet reconnected but that are advected by inflows toward the center of the decoupling region or magnetic field lines that have just reconnected and are moving away following the outflows. Indeed, we observe in simulations that, as reconnection starts to act, the reconnected field lines highlighted using $|\varkappa|$ are those with the the largest jump of ς, with respect to that of several hundreds of randomly generated lines. Furthermore, the value of the jump of these highlighted lines increases with time, that is, as reconnection proceeds.

4.3. Latitudinal Distribution of the Reconnection Processes

In Figure 6 regions with large values of $|\varkappa|$ are shown as red surfaces for simulation B at $t = 460$. These active regions are all located in the upper part of the latitude band affected by the vortex structures, that is, northward with respect to the location where vortices are most intense. With respect to the vortex axis, active regions appear as large sheets in correspondence to the hyperbolic points of the KH velocity field ("a." arrow) or as small-scale filamentary structures aligned with the local magnetic field direction at the northernmost rippled boundary of the vortices ("b." arrow). We recall here that the hyperbolic points are located in between vortices. These sites are also called, in particular in observational papers, the *trailing edges* of KH vortices.

When thought of in the frame of past works on the topic, these reconnection regions at the hyperbolic point may be associated with either Type I or midlatitude reconnection, since both can occur there even if at different latitudes. However, the usual distinction between both types of reconnection loses its meaning when reconnection occurs over a large range of latitudes as observed here. We also note that the reconnecting regions appear as rather continuous patches from the latitude where vortices are most intense to the northernmost end of the region affected by the KH instability. The only distinction concerns the mechanism by which reconnection is driven, that is, how the current is enhanced. At the location where the vortices are most intense the magnetic shear grows mainly due to lateral compression, while in the northern regions it increases mainly because of the magnetic field bending due to differential advection.

For determining which mechanism is at work at different latitudes, we look at the temporal evolution of the reconnected component of the magnetic field and compare it to the evolution of the velocity field generated by the KHI. The reconnected component is defined as $B_{\mathrm{rec}} = \nabla\varsigma/|\nabla\varsigma| \cdot \mathbf{B}$, the component normal to the ς isosurfaces. This quantity generalizes the x component of the magnetic field created by the linear evolution of Tearing instability in a 2-D configuration with an equilibrium field given by $B_{0,y} = B_0 \tanh(x/l)$, described by eigenfunctions of the form $B_{x,k}(x, y, t) = \tilde{B}_{x,k}(x)e^{iky}e^{\gamma_k t}$ (Faganello, Califano, Pegoraro, & Andreussi, 2012).

In Figure 7 we show $|u_x|$ (left) and $|B_{\mathrm{rec}}|$ (right) as a function of z and t for run B. Both quantities have been averaged over x and y; $|u_x|$ gives a precise view on how and where the KHI grows, and in particular it develops a peak at $z = -70$, in the Southern Hemisphere as already stressed in the previous section. $|B_{\mathrm{rec}}|$ has the same peak at $z = -70$ but also a long *summit ridge* going from the main peak to a secondary one at $z = 48$. The main peak corresponds to Type I VIR, indeed it is at the same location of the maximum of u_x that compresses the original sheet. The secondary peak is related to a midlatitude reconnection mechanism: Independently from its actual latitude, it develops far from the location where the vortices are intense, at the latitude where the current is enhanced by differential advection only.

Type I reconnection is characterized by the fact the KH growth rate dictates the growth rate of reconnection (Chen et al., 1997; Knoll & Chacón, 2002; Nakamura et al., 2006), up to the early nonlinear phase. This is shown in Figure 8 where the amplitudes of the $m = 2$ mode (the KH FGM) of u_x (blue continuous lines) and B_{rec} (blue dot-dashed lines) are drawn as a function of time for $z = -70$. The reconnected component follows that of the velocity up to $t = 400$, with a growth rate comparable with the KH one $\simeq 0.03$. On the contrary midlatitude reconnection at $z = 48$ starts at a later time in the nonlinear phase and proceeds at a rate that is really different from that of u_x there, as shown by red lines.

Regarding the elongated reconnection regions, they are related to a small-scale rippling of the magnetopause, with a wave vector nearly perpendicular to the local magnetic field. This rippling appears at the northern edge of the region affected by the vortices, and we conjecture that it is related to a secondary instability that develops during vortex pairing, namely, the secondary KH instability (Cowee et al., 2009; Matsumoto & Seki, 2010; Tenerani et al., 2011) or Type II magnetic reconnection, that is, reconnection related to the folding

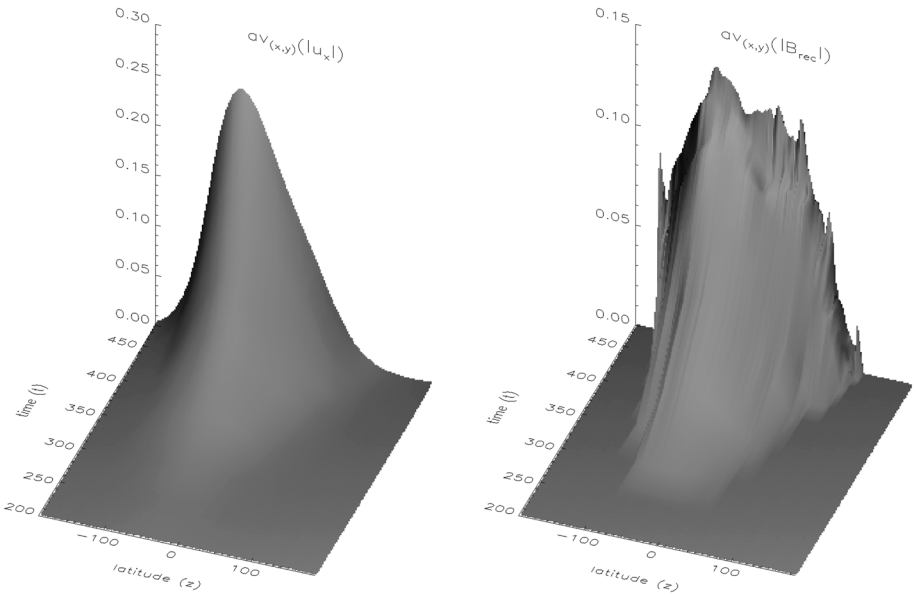

Figure 7. (left) $|u_x|$ averaged over x and y as a function of z and t. (right) $|B_{rec}|$ averaged over x and y as a function of z and t.

of the flow-aligned component of the magnetic field that occurs during the pairing (Faganello et al., 2008b, 2009). In the former case it would be the velocity perturbations caused by the local ideal instability to cause reconnection (Tenerani et al., 2011). In the latter it would be reconnection itself to cause the plasma motion and thus the rippling. The detailed analysis of secondary instabilities and induced reconnection is beyond the scope of this paper and will be tackled in a future work. Nevertheless, contrary to what is observed in 3-D simulations neglecting high-latitude stabilization (Nakamura & Daughton, 2014; Nakamura et al., 2013), in our simulations secondary instabilities occur far away from the region where the primary KH vortices are more intense.

4.4. Double Reconnection Processes

We define double-reconnected field lines as those lines that undergo reconnection twice at different latitudes. About half of these lines connect the magnetosheath in the equatorial region to the magnetospheric plasma at high latitudes (and viceversa). They are particularly important, as compared to once-reconnected lines that simply *open* the magnetopause (allowing for the development of an open LLBL) because they can effectively trap solar wind plasma onto closed field lines of the magnetosphere. Indeed, the flux tubes associated to

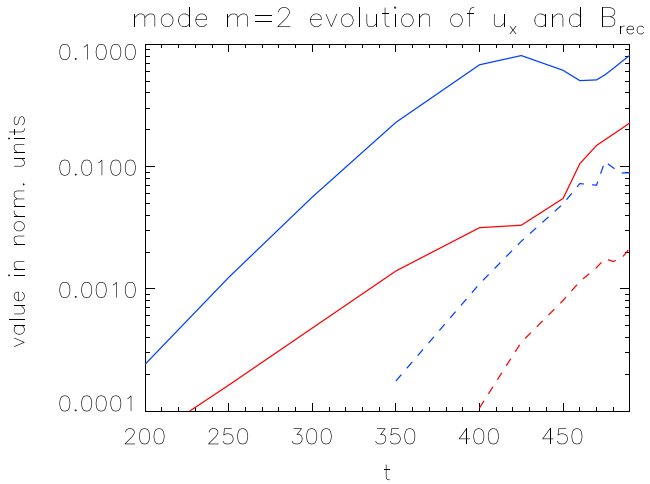

Figure 8. Time evolution of the magnitude of the $m = 2$ mode of u_x at $z = -70$ (blue continuous line) and $z = 48$ (red continuous line) and of B_{rec} at $z = -70$ (blue dot-dashed line) and $z = 48$ (red dot-dashed line).

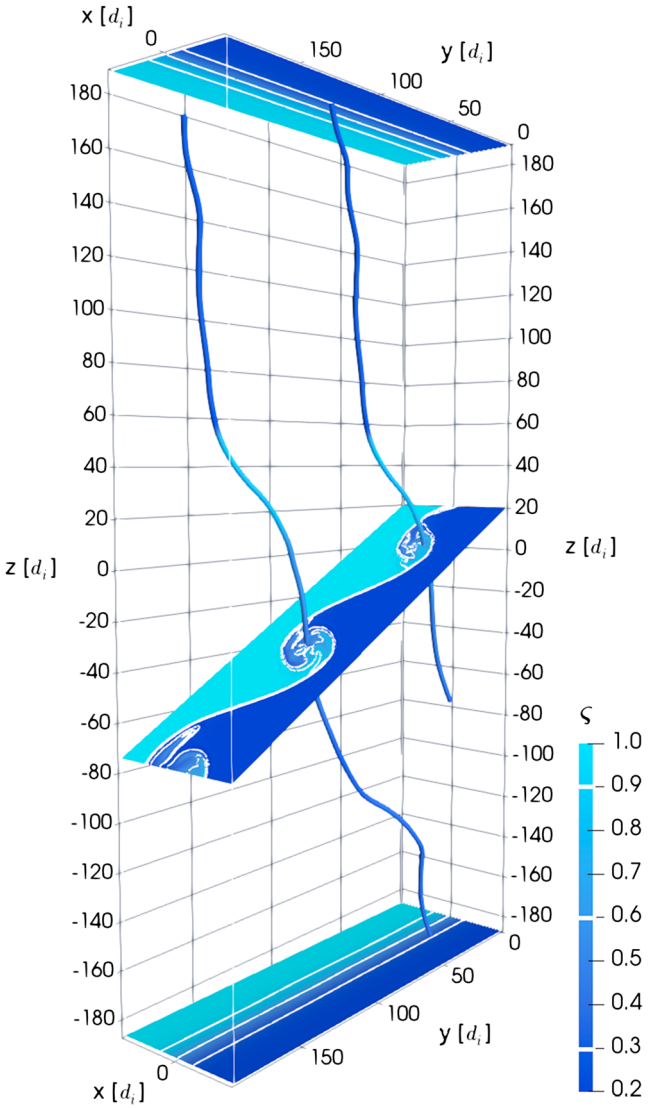

Figure 9. Shaded isosurface ($\varsigma = 0.6$) corresponding to the magnetopause and dark/light blue colors corresponding to the magnetospheric/magnetosheath plasmas for $\tan\varphi = 1.0$ at $t = 460$. The white isocontours correspond to the passive tracer values $\varsigma = 0.3, 0.6, 0.9$. Magnetic field lines are colored using the local value of ς. Note that for easing the visualization the box has been doubled along the *y* direction.

these lines can be considered as new magnetospheric flux tubes with their low-latitude portion populated by solar wind particles. Also, the creation of double-reconnected flux tubes can explain the increase of the specific entropy of the cold ion population measured just inside the magnetopause (Johnson & Wing, 2009). Indeed, a statistical survey of the low-latitude magnetosphere during northward periods shows that the cold dense population of the magnetosheath leaks through the magnetopause increasing its specific entropy by a factor 5–20.

In the absence of a preexisting shear between the IMF and the magnetospheric field double reconnection involves two locations along the same field line in the two opposite hemispheres, acting in the Northern Hemisphere as well as in the Southern Hemisphere in a nearly symmetric way. Adding a magnetic shear to the system not only breaks the symmetry but changes where and how reconnection develops. Recent MMS data show that reconnection occurs in the region where the vortices are observed and also far away from the vortex location, possibly at midlatitude (Vernisse et al., 2016). Our simulations confirm this scenario, showing that for a positive magnetic shear angle ($\tan\varphi > 0$) reconnection occurs at the place where the vortices are most intense and almost simultaneously in regions that are northern that this latitude (the opposite is true for

a negative magnetic shear angle, $\tan\varphi < 0$). In addition our simulations show that double-reconnected lines are generated during the late nonlinear phase of the vortex dynamics for both $\tan\varphi = 0.3$ and $\tan\varphi = 1.0$. An example of these lines is shown in Figure 9 where lines are connected to the dark magnetosphere at high latitudes while crossing the light blue magnetosheath plasma in the central part of the box.

5. Conclusions

We have investigated the development of the KH instability and the induced reconnection processes in a geometry that models the configuration of the flanks of the Earth's magnetosphere during periods of northward IMF by means of high-resolution two-fluid simulations. Our initial configuration takes into account both the effect of high-latitude stabilization and of a preexisting magnetic shear between the magnetospheric and the magnetosheath fields. The most remarkable features of the plasma dynamics observed in this configuration are the latitude location where the KH instability grows more vigorously, the place where induced magnetic reconnection occurs and the mechanism underlying induced reconnection.

Concerning the first point, as soon as the IMF has a component along the flow (described by a shear angle φ in our simulations) the reflection symmetry about the equatorial plane is broken even if the density, temperature, and velocity field are symmetric (the northward component of the magnetic field is symmetric too). In particular, we have shown that KH vortices develop asymmetrically with respect to the equatorial plane depending on the sign of the pseudoscalar $\mathbf{\Omega}_0 \cdot \mathbf{J}_0$, where $\mathbf{J}_0$ is the equilibrium current associated to the rotation of the equilibrium magnetic field across the magnetopause and $\mathbf{\Omega}_0$ is the equilibrium vorticity associated to the velocity shear. When $\mathbf{\Omega}_0 \cdot \mathbf{J}_0 > 0$, KH vortices fully develop mainly in the Southern Hemisphere, whereas the contrary is true for $\mathbf{\Omega}_0 \cdot \mathbf{J}_0 < 0$.

From a physical point of view the shift of the vortices toward one hemisphere can be explained by looking at the dynamics of magnetic field lines at the beginning of the nonlinear phase. In fact, even if the linear KH growth rate is symmetric, the dynamics of field lines is not. Indeed, the magnetic field lines are frozen in the plasma fluid motion and are advected differently at high latitudes, where the magnetospheric/solar wind velocity stays unperturbed, and at low latitude where the instability develops. This differential advection causes the averaged magnetic field shear to increase in one hemisphere and to be reduced in the other one. Since the magnetic shear tends to inhibit the KH growth, vortices develop asymmetrically.

Since both $\mathbf{\Omega}_0$ and $\mathbf{J}_0$ change sign when passing from the magnetospheric dusk flank to the dawn flank, the hemisphere where the vortices are more intense is the same at both flanks, for example, the southern one if the flow-aligned component of the IMF is positive. This fact can be directly inferred from the symmetry properties of the system: The dawn flank configuration can be obtained from the dusk one by reflecting the system with respect to the magnetopause and applying charge conjugation. Since MHD equations are invariant under *reflection + charge conjugation*, the large-scale KH dynamics is specular.

In the past, Farrugia et al. (1998) and Gratton et al. (2003) considered the impact of the clock angle of the IMF on the KH instability, that is, the impact of a westward component of the magnetic field, perpendicular to both the northward and the flow directions. Neglecting the flow-aligned component of the IMF, they showed that for a positive clock angle the location of the maximum linear growth rate of the KH instability is located in the Northern Hemisphere at the duskside. The opposite is true at the dawn flank so that the most unstable hemispheres are different at the dawnside/duskside. This behavior has been obtained by looking at the configuration of the magnetic field close to the global magnetopause, taking into account the dipolar configuration of the magnetospheric field and the draping of the solar wind magnetic field around the magnetopause as described by a global MHD code. From a symmetry point of view this fact is not surprising since as soon as a westward component of the magnetic field is considered the global system is no more invariant under reflection + charge conjugation so that the dawn and dusk large-scale dynamics are not specular (here the reflection of the global system is about the plane defined by solar wind direction and the northward direction, passing through the Earth).

In our configuration the clock angle is not included so that the nonlinear KH activity at the flanks is specular. On the contrary when considering the clock angle but neglecting the shear angle (Gratton et al., 2003; Farrugia et al., 1998) the linear dynamics is antispecular. Taking into account both the shear angle and the clock angle effect would help in clarifying satellite data analysis, in particular when KH activities measured at both flanks (at different latitudes) are compared (Hasegawa et al., 2006; Nishino et al., 2011; Taylor et al., 2012).

The magnetic shear angle has a similar but opposite impact on the location where reconnection occurs, with respect to the location where the KH vortices eventually settle, since reconnection develops faster in regions where the magnetic shear is larger. The local magnetic shear is enhanced in two different ways during the nonlinear dynamics. The first one is the pinching of the preexisting current sheet that occurs at the hyperbolic point (in between successive vortices) of the KH velocity field, as in Type I reconnection. The second one is the modification of the preexisting current sheet far away from the location where vortices are intense due to differential advection and field line bending. The local magnetic shear becomes larger in the hemisphere opposite to the one where KH vortices are more developed, that is, in the Northern (Southern) Hemisphere for a positive (negative) $\mathbf{\Omega}_0 \cdot \mathbf{J}_0$. Both mechanisms are at work in our simulations, leading to the development of reconnection in a wide latitude range: from the location where vortices are most intense to the upper (lower) edge of the region affected by KH perturbations.

Recent MMS observations on 8 September 2015 suggest that Type I reconnection proceeds nearby vortices (Eriksson et al., 2016) and that, at the same time, remote reconnection occurs probably at midlatitudes (Vernisse et al., 2016). The simulations discussed here reproduce this dynamics and further suggest that remote reconnection should be favored in a given hemisphere depending on the initial magnetic shear (i.e., the prevailing IMF orientation). In particular when the flow-aligned component of the IMF is negative, as during this peculiar MMS observations, the favored hemisphere is the southern one. This is compatible with the fact that the number of remote reconnection events observed on this day by MMS is bigger in the Southern Hemisphere than in the Northern Hemisphere (Vernisse et al., 2016).

Our simulations also show that reconnection, going on at different latitudes, is able to produce double-reconnected magnetic field lines connected to the Earth and thus to trap dense magnetosheath plasma inside the magnetopause even when a significant magnetic shear is present in the initial configuration. These results indicate that this double reconnection process associated with KH vortices is a viable mechanism to explain the formation of the flank LLBL even in the presence of significant magnetic shear. Future work shall focus on determining the efficiency of this mechanism as a function of the initial magnetic shear.

Acknowledgments
The simulations presented here have been performed at CINECA (Bologna, Italy) under the ISCRA allocation initiative. The necessary information (plasma model, starting equilibrium, numerical schemes adopted in the code) for reproducing the simulation results discussed here is clearly written in the article.

References

Adamson, E., Nykyri, K., & Otto, A. (2016). The Kelvin-Helmholtz instability under Parker-Spiral interplanetary magnetic field conditions at the magnetospheric flanks. *Advances in Space Research*, *58*(2), 218–230. https://doi.org/10.1016/j.asr.2015.09.013

Andreussi, T., Morrison, P. J., & Pegoraro, F. (2012). Hamiltonian magnetohydrodynamics: Helically symmetric formulation, Casimir invariants, and equilibrium variational principles. *Physics of Plasmas*, *19*(5), 052102. https://doi.org/10.1063/1.4714761

Birn, J., Drake, J. F., Shay, M. A., Rogers, B. N., Denton, R. E., Hesse, M., et al. (2001). Geospace Environmental Modeling (GEM) magnetic reconnection challenge. *Journal of Geophysical Research*, *106*, 3715–3720. https://doi.org/10.1029/1999JA900449

Borgogno, D., Califano, F., Faganello, M., & Pegoraro, F. (2015). Double-reconnected magnetic structures driven by Kelvin-Helmholtz vortices at the Earth's magnetosphere. *Physics of Plasmas*, *22*(3), 032301. https://doi.org/10.1063/1.4913578

Cerri, S. S., Henri, P., Califano, F., Del Sarto, D., Faganello, M., & Pegoraro, F. (2013). Extended fluid models: Pressure tensor effects and equilibria. *Physics of Plasmas*, *20*(11), 112112. https://doi.org/10.1063/1.4828981

Chandrasekhar, S. (1961). *Hydrodynamic and hydrodynamic stability*. Oxford: Clarendon Press. OUP.

Chaston, C. C., Wilber, M., Mozer, F. S., Fujimoto, M., Goldstein, M. L., Acuna, M., et al. (2007). Mode conversion and anomalous transport in Kelvin-Helmholtz vortices and kinetic Alfvén waves at the Earth's magnetopause. *Physical Review Letters*, *99*(17), 175004. https://doi.org/10.1103/PhysRevLett.99.175004

Chen, Q., Otto, A., & Lee, L. C. (1997). Tearing instability, Kelvin-Helmholtz instability, and magnetic reconnection. *Journal of Geophysical Research*, *102*, 151–162. https://doi.org/10.1029/96JA03144

Cowee, M. M., Winske, D., & Gary, S. P. (2009). Two-dimensional hybrid simulations of superdiffusion at the magnetopause driven by Kelvin-Helmholtz instability. *Journal of Geophysical Research*, *114*, A10209. https://doi.org/10.1029/2009JA014222

De Camillis, S., Cerri, S. S., Califano, F., & Pegoraro, F. (2016). Pressure anisotropy generation in a magnetized plasma configuration with a shear flow velocity. *Plasma Physics and Controlled Fusion*, *58*(4), 045007. https://doi.org/10.1088/0741-3335/58/4/045007

Drazin, P. G., & Reid, W. H. (1981). Hydrodynamic stability (*NASA STI/Recon Technical Report A, 82*, 17950).

Dungey, J. W. (1961). Interplanetary magnetic field and the auroral zones. *Physical Review Letters*, *6*(2), 47.

Eriksson, S., Lavraud, B., Wilder, F. D., Stawarz, J. E., Giles, B. L., Burch, J. L., et al. (2016). Magnetospheric multiscale observations of magnetic reconnection associated with Kelvin-Helmholtz waves. *Geophysical Research Letters*, *43*, 5606–5615. https://doi.org/10.1002/2016GL068783

Faganello, M., & Califano, F. (2017). Magnetized Kelvin-Helmholtz instability: Theory and simulations in the Earth's magnetosphere context. *Journal of Plasma Physics*, *83*(6), 68. https://doi.org/10.1017/S0022377817000770

Faganello, M., Califano, F., & Pegoraro, F. (2008a). Competing mechanisms of plasma transport in inhomogeneous configurations with velocity shear: The solar-wind interaction with Earth's magnetosphere. *Physical Review Letters*, *100*(1), 015001. https://doi.org/10.1103/PhysRevLett.100.015001

Faganello, M., Califano, F., & Pegoraro, F. (2008b). Numerical evidence of undriven, fast reconnection in the solar-wind interaction with Earth's magnetosphere: Formation of electromagnetic coherent structures. *Physical Review Letters*, *101*(10), 105001. https://doi.org/10.1103/PhysRevLett.101.105001

Faganello, M., Califano, F., & Pegoraro, F. (2008c). Time window for magnetic reconnection in plasma configurations with velocity shear. *Physical Review Letters*, *101*(17), 175003. https://doi.org/10.1103/PhysRevLett.101.175003

Faganello, M., Califano, F., & Pegoraro, F. (2009). Being on time in magnetic reconnection. *New Journal of Physics*, *11*(6), 063008. https://doi.org/10.1088/1367-2630/11/6/063008

Faganello, M., Califano, F., Pegoraro, F., & Andreussi, T. (2012). Double mid-latitude dynamical reconnection at the magnetopause: An efficient mechanism allowing solar wind to enter the Earth's magnetosphere. *EPL (Europhysics Letters)*, *100*(6), 69001. https://doi.org/10.1209/0295-5075/100/69001

Faganello, M, Califano, F, Pegoraro, F, Andreussi, T, & Benkadda, S (2012). Magnetic reconnection and Kelvin-Helmholtz instabilities at the Earth's magnetopause. *PPlasma Physics and Controlled Fusion*, *54*(12), 124037. https://doi.org/10.1088/0741-3335/54/12/124037

Faganello, M., Califano, F., Pegoraro, F., & Retinò, A. (2014). Kelvin-Helmholtz vortices and double mid-latitude reconnection at the Earth's magnetopause: Comparison between observations and simulations. *EPL (Europhysics Letters)*, *107*(1), 19001. https://doi.org/10.1209/02955075/107/19001

Farrugia, C. J., Gratton, F. T., Bender, L., Biernat, H. K., Erkaev, N. V., Quinn, J. M., et al. (1998). Charts of joint Kelvin-Helmholtz and Rayleigh-Taylor instabilites at the dayside magnetopause for strongly northward interplanetary magnetic field. *Journal of Geophysical Research*, *103*, 6703–6728. https://doi.org/10.1029/97JA03248

Fuselier, S. A., Anderson, B. J., & Onsager, T. G. (1995). Particle signatures of magnetic topology at the magnetopause: AMPTE/CCE observations. *Journal of Geophysical Research*, *100*, 11,805–11,821. https://doi.org/10.1029/94JA02811

Gosling, J. T., Thomsen, M. F., Bame, S. J., Elphic, R. C., & Russell, C. T. (1991). Observations of reconnection of interplanetary and lobe magnetic field lines at the high-latitude magnetopause. *Journal of Geophysical Research*, *96*, 14,097–14,106. https://doi.org/10.1029/91JA01139

Gratton, F. T., Gnavi, G., Farrugia, C. J., & Bender, L. (2003). The stability of the pristine magnetopause. *Planetary Space Science*, *51*, 769–783. https://doi.org/10.1016/S00320633(03)00113-2

Hasegawa, H., Fujimoto, M., Takagi, K., Saito, Y., Mukai, T., & RèMe, H. (2006). Single-spacecraft detection of rolled-up Kelvin-Helmholtz vortices at the flank magnetopause. *Journal of Geophysical Research*, *111*, A09203. https://doi.org/10.1029/2006JA011728

Hasegawa, H., Retinò, A., Vaivads, A., Khotyaintsev, Y., André, M., Nakamura, T. K. M., et al. (2009). Kelvin-Helmholtz waves at the Earth's magnetopause: Multiscale development and associated reconnection. *Journal of Geophysical Research*, *114*, A12207. https://doi.org/10.1029/2009JA014042

Hedstrom, G. W. (1979). Nonreflecting boundary conditions for nonlinear hyperbolic systems. *Journal of Computational Physics*, *30*, 222–237. https://doi.org/10.1016/0021-9991(79)901001

Henri, P., Cerri, S. S., Califano, F., Pegoraro, F., Rossi, C., Faganello, M., et al. (2013). Nonlinear evolution of the magnetized Kelvin-Helmholtz instability: From fluid to kinetic modeling. *Physics of Plasmas*, *20*(10), 102118. https://doi.org/10.1063/1.4826214

Johnson, J. R., & Cheng, C. Z. (2001). Stochastic ion heating at the magnetopause due to kinetic Alfvén waves. *Geophysical Research Letters*, *28*, 4421–4424. https://doi.org/10.1029/2001GL013509

Johnson, J. R., Cheng, C. Z., & Song, P. (2001). Signatures of mode conversion and kinetic Alfvén waves at the magnetopause. *Geophysical Research Letters*, *28*, 227–230. https://doi.org/10.1029/2000GL012048

Johnson, J. R., & Wing, S. (2009). Northward interplanetary magnetic field plasma sheet entropies. *Journal of Geophysical Research*, *114*, A00D08. https://doi.org/10.1029/2008JA014017

Knoll, D. A., & Brackbill, J. U. (2002). The Kelvin-Helmholtz instability, differential rotation, and three-dimensional, localized, magnetic reconnection. *Physics of Plasmas*, *9*(9), 3775–3782. https://doi.org/10.1063/1.1494070

Knoll, D. A., & Chacón, L. (2002). Magnetic reconnection in the two-dimensional Kelvin-Helmholtz instability. *Physical Review Letters*, *88*(21), 215003. https://doi.org/10.1103/PhysRevLett.88.215003

Labelle, J., & Treumann, R. A. (1988). Plasma waves at the dayside magnetopause. *Space Science Reviews*, *47*, 175–202. https://doi.org/10.1007/BF00223240

Landi, S., Velli, M., & Einaudi, G. (2005). Alfvén waves and shock wave formation at an X-point magnetic field configuration. *The Astrophysical Journal*, *624*, 392–401. https://doi.org/10.1086/428822

Lavraud, B., Thomsen, M. F., Lefebvre, B., Schwartz, S. J., Seki, K., Phan, T. D., et al. (2006). Evidence for newly closed magnetosheath field lines at the dayside magnetopause under northward IMF. *Journal of Geophysical Research*, *111*, A05211. https://doi.org/10.1029/2005JA011266

Le, G., Russell, C. T., & Gosling, J. T. (1994). Structure of the magnetopause for low Mach number and strongly northward interplanetary magnetic field. *Journal of Geophysical Research*, *99*, 23,723–23,734. https://doi.org/10.1029/94JA02182

Lele, S. K. (1992). Compact finite difference schemes with spectral-like resolution. *Journal of Computational Physics*, *103*, 16–42. https://doi.org/10.1016/0021-9991(92)90324-R

Liu, Z. X., & Hu, Y. D. (1988). Local magnetic reconnection caused by vortices in the flow field. *Geophysical Research Letters*, *15*, 752–755. https://doi.org/10.1029/GL015i008p00752

Matsumoto, Y., & Hoshino, M. (2004). Onset of turbulence induced by a Kelvin-Helmholtz vortex. *Geophysical Research Letters*, *31*, L02807. https://doi.org/10.1029/2003GL018195

Matsumoto, Y., & Seki, K. (2007). The secondary instability initiated by the three-dimensional nonlinear evolution of the Kelvin-Helmholtz instability. *Journal of Geophysical Research*, *112*, A06223. https://doi.org/10.1029/2006JA012114

Matsumoto, Y., & Seki, K. (2010). Formation of a broad plasma turbulent layer by forward and inverse energy cascades of the Kelvin-Helmholtz instability. *Journal of Geophysical Research*, *115*, A10231. https://doi.org/10.1029/2009JA014637

Mitchell, D. G., Kutchko, F., Williams, D. J., Eastman, T. E., & Frank, L. A. (1987). An extended study of the low-latitude boundary layer on the dawn and dusk flanks of the magnetosphere. *Journal of Geophysical Research*, *92*, 7394–7404. https://doi.org/10.1029/JA092iA07p07394

Miura, A. (1997). Compressible magnetohydrodynamic Kelvin-Helmholtz instability with vortex pairing in the two-dimensional transverse configuration. *Physics of Plasmas*, *4*, 2871–2885. https://doi.org/10.1063/1.872419

Nakamura, T. K. M., & Daughton, W. (2014). Turbulent plasma transport across the Earth's low-latitude boundary layer. *Geophysical Research Letters*, *41*, 8704–8712. https://doi.org/10.1002/2014GL061952

Nakamura, T. K. M., Daughton, W., Karimabadi, H., & Eriksson, S. (2013). Three-dimensional dynamics of vortex-induced reconnection and comparison with THEMIS observations. *Journal of Geophysical Research: Space Physics*, *118*, 5742–5757. https://doi.org/10.1002/jgra.50547

Nakamura, T. K. M., Fujimoto, M., & Otto, A (2006). Magnetic reconnection induced by weak Kelvin-Helmholtz instability and the formation of the low-latitude boundary layer. *Geophysical research letters*, *33*, L14106. https://doi.org/10.1029/2006GL026318

Nakamura, T. K. M., Hayashi, D., Fujimoto, M., & Shinohara, I. (2004). Decay of MHD-scale Kelvin-Helmholtz vortices mediated by parasitic electron dynamics. *Physical Review Letters*, *92*(14), 145001. https://doi.org/10.1103/PhysRevLett.92.145001

Nishino, M. N., Hasegawa, H., Fujimoto, M., Saito, Y., Mukai, T., Dandouras, I., et al. (2011). A case study of Kelvin-Helmholtz vortices on both flanks of the Earth's magnetotail. *Planetary Space Science*, *59*, 502–509. https://doi.org/10.1016/j.pss.2010.03.011

Nykyri, K., Otto, A., Lavraud, B., Mouikis, C., Kistler, L. M., Balogh, A., & Rème, H. (2006). Cluster observations of reconnection due to the Kelvin-Helmholtz instability at the dawnside magnetospheric flank. *Annales Geophysicae*, *24*, 2619–2643. https://doi.org/10.5194/angeo-242619-2006

Onsager, T. G., Scudder, J. D., Lockwood, M., & Russell, C. T. (2001). Reconnection at the high-latitude magnetopause during northward interplanetary magnetic field conditions. *Journal of Geophysical Research*, *106*(A11), 25,467–25,488. https://doi.org/10.1029/2000JA000444

Otto, A., & Fairfield, D. H. (2000). Kelvin-Helmholtz instability at the magnetotail boundary: MHD simulation and comparison with Geotail observations. *Journal of Geophysical Research*, *105*, 21,175–21,190. https://doi.org/10.1029/1999JA000312

Song, P., & Russell, C. T. (1992). Model of the formation of the low-latitude boundary layer for strongly northward interplanetary magnetic field. *Journal of Geophysical Research*, *97*, 1411–1420. https://doi.org/10.1029/91JA02377

Sonnerup, B. U. O. (1980). Theory of the low-latitude boundary layer. *Journal of Geophysical Research*, *85*, 2017–2026. https://doi.org/10.1029/JA085iA05p02017

Southwood, D. J. (1968). The hydromagnetic stability of the magnetospheric boundary. *Planetary Space Science*, *16*, 587–605. https://doi.org/10.1016/0032-0633(68)90100-1

Taylor, M. G. G. T., Hasegawa, H., Lavraud, B., Phan, T., Escoubet, C. P., Dunlop, M. W., et al. (2012). Spatial distribution of rolled up Kelvin-Helmholtz vortices at Earth's dayside and flank magnetopause. *Annales Geophysicae*, *30*, 1025–1035. https://doi.org/10.5194/angeo-30-1025-2012

Tenerani, A., Faganello, M., Califano, F., & Pegoraro, F. (2011). Nonlinear vortex dynamics in an inhomogeneous magnetized plasma with a sheared velocity field. *Plasma Physics and Controlled Fusion*, *53*(1), 015003. https://doi.org/10.1088/0741-3335/53/1/015003

Terasawa, T., Fujimoto, M., Mukai, T., Shinohara, I., Saito, Y., Yamamoto, T., et al. (1997). Solar wind control of density and temperature in the near-Earth plasma sheet: WIND/GEOTAIL collaboration. *Geophysical research letters*, *24*(8), 935–938.

Thompson, K. W. (1990). Time-dependent boundary conditions for hyperbolic systems. II. *Journal of Computational Physics*, *89*, 439–461. https://doi.org/10.1016/0021-9991(90)90152-Q

Vernisse, Y., Lavraud, B., Eriksson, S., Gershman, D. J., Dorelli, J., Pollock, C., et al. (2016). Signatures of complex magnetic topologies from multiple reconnection sites induced by Kelvin-Helmholtz instability. *Journal of Geophysical Research: Space Physics*, *121*, 9926–9939. https://doi.org/10.1002/2016JA023051

Walker, A. D. M. (1981). The Kelvin-Helmholtz instability in the low-latitude boundary layer. *Planetary Space Science*, *29*, 1119–1133. https://doi.org/10.1016/0032-0633(81)90011-8

Winant, C. D., & Browand, F. K. (1974). Vortex pairing: The mechanism of turbulent mixing-layer growth at moderate Reynolds number. *Journal of Fluid Mechanics*, *63*, 237–255. https://doi.org/10.1017/S0022112074001121